Hindawi
International Transactions on Electrical Energy Systems
Volume 2023, Article ID 9789630, 1 page
https://doi.org/10.1155/2023/9789630

Retraction

Retracted: Simulation of Flow-Induced Vibration and Dynamic Performance of Circular-Arc Helical Gear Pump under Background of Machine Learning

International Transactions on Electrical Energy Systems

Received 28 November 2023; Accepted 28 November 2023; Published 29 November 2023

This article has been retracted by Hindawi, as publisher, following an investigation undertaken by the publisher [1]. This investigation has uncovered evidence of systematic manipulation of the publication and peer-review process. We cannot, therefore, vouch for the reliability or integrity of this article.

Please note that this notice is intended solely to alert readers that the peer-review process of this article has been compromised.

Wiley and Hindawi regret that the usual quality checks did not identify these issues before publication and have since put additional measures in place to safeguard research integrity.

We wish to credit our Research Integrity and Research Publishing teams and anonymous and named external researchers and research integrity experts for contributing to this investigation.

The corresponding author, as the representative of all authors, has been given the opportunity to register their agreement or disagreement to this retraction. We have kept a record of any response received.

References

[1] X. Wei, Y. Feng, X. Han, and Z. He, "Simulation of Flow-Induced Vibration and Dynamic Performance of Circular-Arc Helical Gear Pump under Background of Machine Learning," *International Transactions on Electrical Energy Systems*, vol. 2022, Article ID 9513357, 10 pages, 2022.

Hindawi
International Transactions on Electrical Energy Systems
Volume 2022, Article ID 9513357, 10 pages
https://doi.org/10.1155/2022/9513357

Research Article

Simulation of Flow-Induced Vibration and Dynamic Performance of Circular-Arc Helical Gear Pump under Background of Machine Learning

Xiaoling Wei, Yongbao Feng, Xiaoxia Han, and Zhenxin He

Department of Missile Engineering, PLA Rocket Force University of Engineering, Xi'an 710025, Shaanxi, China

Correspondence should be addressed to Yongbao Feng; fyb1213@sina.com

Received 25 August 2022; Revised 16 September 2022; Accepted 21 September 2022; Published 4 October 2022

Academic Editor: Nagamalai Vasimalai

At present, with the continuous development and great improvement of mechanical manufacturing, processing, and assembly technology, mechanical flow-induced vibration (FIV) with a relatively concentrated frequency domain can be controlled by active and passive noise reduction methods. However, whether it is active noise reduction or passive noise reduction, they all focus on how to suppress the transmission of sound waves and cannot solve the problems of flow leakage, obvious temperature rise, and noise excitation from the root cause. Therefore, it is necessary to determine the location of the primary and secondary excitation sound sources of FIV, the identification of true and false sounds, and the characteristic relationship between flow and noise. This provides a theoretical basis and engineering application direction for the mechanism of noise reduction of FIV. The numerical calculation part of the acoustics in this paper is solved by the hybrid method, and the flow field is discretely calculated by the large eddy simulation (LES) module in the Fluent software. When the calculated flow field is stable, the velocity field of one impeller rotation period is selected to be output as the iterative value of the sound field and imported into ACTRAN for Fourier transform. Then, the sound field calculation is carried out, and the result of the spatial and temporal variation of the sound field is finally obtained. Through experiments, it was found that when the load of the gear pump is 8 MPa, the volumetric efficiency of the optimized circular-arc helical gear pump of the sliding bearing was improved by about 4%. When the rotation speed is 2100°r/min, the arc helical gear pump reduced the surface temperature rise by 2.5°C. This verified that the optimized performance of the sliding bearing in the arc helical gear pump is significantly improved. Through the theoretical model of the temperature rise of the sliding bearing, the phenomenon that the surface temperature of the prototype gear pump was not significantly increased with the loading in the low pressure region is explained.

1. Introduction

A pump is a device that can convert mechanical energy into pumping fluid energy. Usually, the motor drives the impeller to rotate through the rotation of the pump shaft, and the fluid generates energy after the impeller rotates to do work, so as to meet the conveying conditions required by the user. The pump acts as an energy conversion and fluid delivery device. It is widely used in all walks of life, such as in daily life, or in agriculture, industry, and military fields. According to statistics, the power consumption of pumps accounts for more than 15% of the total power generation. When the fluid medium is transported, due to the influence of the fluid viscosity, there are many complex flow structures in the flow field of the centrifugal pump at the same time. For example, in the region of the impeller outlet near the trailing edge of the blade, a "low energy zone" would appear on the back of the blade. The flow through this side is stable and is referred to as a "wake" structure. In the face of the "high pressure area," the flow is unstable, called "jet" structure, which increases the velocity gradient and intensifies the fluid energy exchange, thereby affecting the mainstream flow. Therefore, if a violent and unstable flow occurs in the internal flow field and the flow deviates from the design condition, it is easy to cause high-decibel noise and large-scale vibration, thereby shortening the service life of the

pump and aggravating noise pollution. In the early days, due to the limitation of computer design level, it was difficult for researchers to perform direct numerical simulation of complex three-dimensional flow. This largely relies on experimental or analytical methods to study flow-induced noise production. Therefore, in order to meet the needs of increasing the bearing life of the industrial system, this paper analyzes the FIV phenomenon of the arc helical gear pump and builds a performance test model of the arc helical gear pump. Through the gear pump temperature rise test experiment, the influence law of load and rotational speed on the gear pump temperature rise is proposed. It proves that the arc helical gear pump can run smoothly under high pressure and high speed compared with other ordinary gear pumps.

The innovation of this paper is that a dynamic performance simulation method of arc helical gear pump is proposed, which provides a new way for the simulation of the gear pump model. This method improves the mechanical efficiency by optimizing the gear pump bearing, which can also increase the service life of the pump. It reduces costs for the use of factory pumps.

2. Related Work

With the expansion of computing power and the improvement and development of machine learning (ML) theory, it has gradually been applied to various leading areas. Buczak and Guven investigated the application of machine learning to analyze network intrusion detection. A short tutorial description of each method was presented [1]. Zhou et al. provided directions for identifying relevant opportunities and challenges for the various stages of ML and components of MLBiD [2]. Kavakiotis et al. conducted a systematic review of the application of machine learning, data mining techniques, and tools in the field of diabetes research, resulting in predictions and diagnosis [3]. It can be seen that machine learning is widely used in network security, industrial machinery, medical, and other fields.

FIV is a common problem in energy systems, so in order to reduce the loss caused by FIV, many scholars have conducted related research. For example, Merzari et al. discussed the use of computational fluid dynamics code Nek5000 coupled with structural code Diablo to simulate flow and associated FIV in a helical coil heat exchanger [4]. Xu et al. studied the dynamic response of smooth cylinders placed either upstream or downstream of a tandem cylinder to improve the understanding of the FIV behavior of a dual tandem cylinder system [5]. Quen et al. conducted experiments on low mass ratio flexible cylinders with two and three initial helical blades. The cylinder can freely vibrate in the in-line and transverse flow directions at subcritical Reynolds numbers [6]. Ren et al. conducted an experimental study of FIV on flexible pipes fitted with spiral slats. The results showed that the suppression efficiency and fatigue damage reduction rate of oscillatory flow are not as ideal as steady flow [7]. Xu et al. conducted an experimental study of two identical elastically mounted cylinders in series in a surface water channel. It was concluded that when the deceleration speed does not exceed 12.0, when $T/D = 2.57$, 3.57, and 4.57, the fly characteristics of the upstream cylinder are similar to that of the single cylinder [8]. In general, their engineering estimation method mainly obtains the parameters in the empirical formula through data regression and considers less structural factors. Although verified by experiments, it is still difficult to guide the FIV design of hydraulic machinery.

3. Simulation of FIV Sliding Bearing in Arc Helical Gear Pump

3.1. Experiment Bench Data Acquisition System. The overall idea and principle of the test software part of the arc helical gear wheel pump in this paper are shown in Figure 1.

It can be seen from Figure 1 that the software part measures the temperature, flow, pressure, speed, and other properties by the sensor and converts it into an analog signal. The data acquisition card is input to the host computer according to the corresponding channel, and the signal acquisition and conversion are completed through software processing [9]. In this paper, LabVIEW software is used for programming to complete the acquisition and result display of temperature, flow, pressure, and rotational speed signals, which can display images or export data.

3.2. Simulation Model of Internal Flow Field of Gear Pump. To carry out simulation analysis, it is necessary to clarify the idea of simulation calculation, conduct a large number of practical calculations, record, analyze, and compare the condition settings and calculation results of each calculation. The simulation calculation of the pressure field is carried out first, and after a certain number of steps are relatively stable, the energy model is turned on, and the simulation calculation of the temperature field is carried out, which is easier to ensure the calculation convergence and stable and smooth progress. The high-pressure high-speed miniaturized helical gear pump designed in this paper has a design speed of 10000 r/min and a pressure of 25 MPa. This paper analyzes the dynamic performance of the internal flow field of a high-pressure high-speed miniaturized arc helical gear pump. 2D simulation cannot simulate axial leakage and pressure. Therefore, the results of the 3D simulation are closer to the true value than the 2D simulation results [10]. In view of the problem of high temperature rise during the operation of the prototype, it is necessary to analyze the influence of the internal fluid of the gear pump on the temperature rise, as shown in Figure 2.

Figure 2 is a flow chart of analyzing the gear pump using Fluent software. In order for the experiment to make the simulation analysis accurate and smooth, it is necessary to clarify the idea of simulation calculation, carry out a large number of practical calculations, record, analyze, and compare the condition settings and calculation results of each calculation [11–13]. The simulation calculation of the pressure field is carried out first, and after a certain number of steps are relatively stable, the energy model is opened, and the simulation calculation of the temperature field is carried

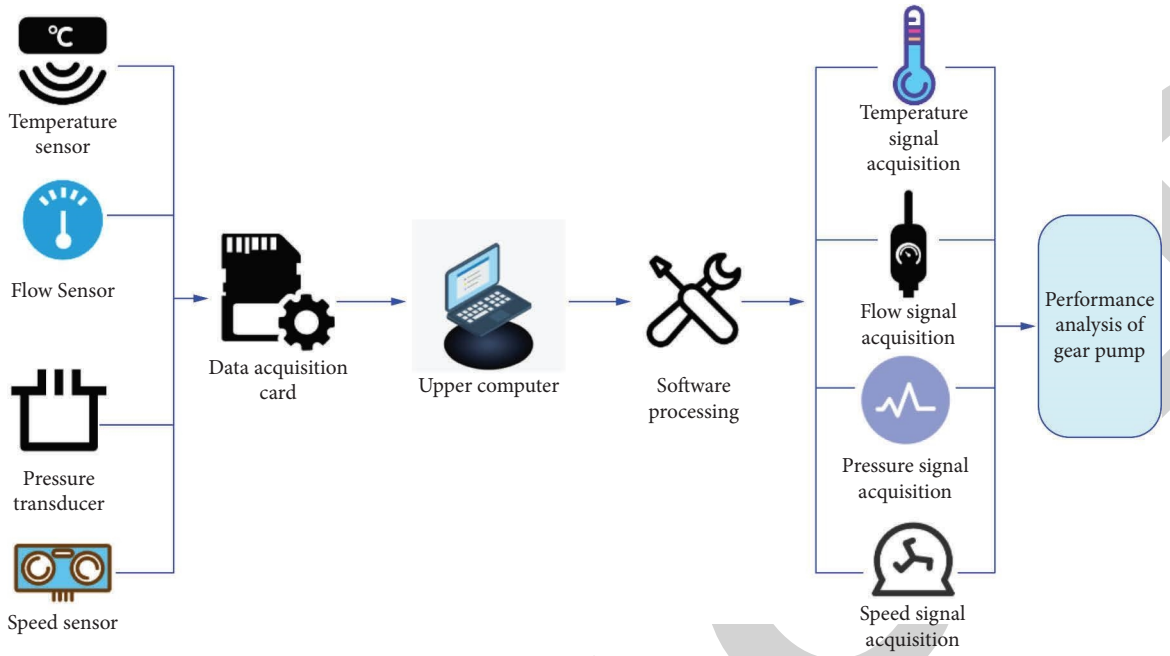

Figure 1: Schematic diagram of the experimental bench software.

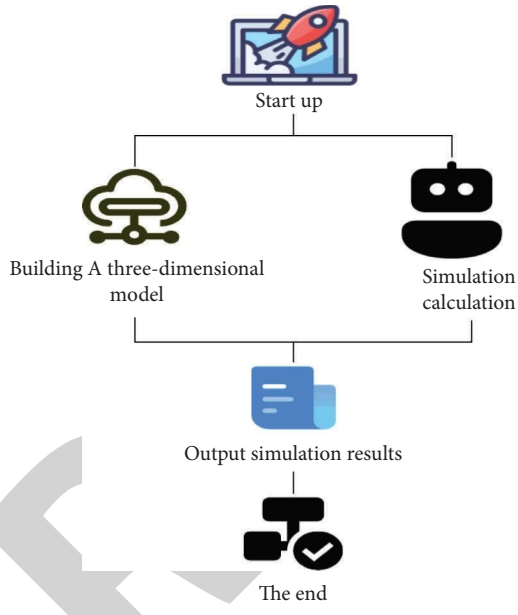

Figure 2: Flow diagram of fluent analysis gear pump flow field.

out. It is easier to ensure the calculation convergence and stable and smooth progress.

3.3. Construction of FIV Model. FIV is the flow-acoustic coupling caused by the unsteady flow of fluid. The sound generation process is very complex, including a quadrupole source in which turbulent fluid participates in sound generation, and a dipole source generated by fluid-structure coupling excitation after the fluid hits the solid wall [14, 15]. Therefore, in the process of numerical simulation, it is necessary to comprehensively consider the actual flow situation and the relevant principles of computational fluid dynamics and select a suitable numerical model to simulate the internal flow field. Compared with direct numerical simulation (DNS) and Reynolds time-averaged simulation (RNS), large eddy simulation is in between. It neither has high requirements on spatial and temporal resolution like DNS nor can it only provide average information of turbulence like RNS, resulting in insufficient description of the flow field. This section mainly introduces the governing equations of large eddy simulation.

The N–S equation for the incompressible constant viscosity coefficient is

$$\frac{\partial u_i}{\partial t} + \frac{\partial u_i u_j}{\partial x_j} = -\frac{1}{\rho}\frac{\partial \rho}{\partial x_i} + \frac{\partial\left(\nu \cdot 2S_{ij}\right)}{\partial x_j}. \tag{1}$$

In the formula, the stretch rate tensor is

$$S_{\mathrm{ij}} = \frac{1}{2}\left(\frac{\partial u_i}{\partial x_j} + \frac{\partial u_j}{\partial x_i}\right). \tag{2}$$

The subscripts $i, j = 1, 2, 3$ and u_i represent the velocity components associated with x_i, ρ is the fluid density, and ν is the fluid's kinematic viscosity coefficient.

In the large eddy simulation, the large and small vortex systems are distinguished by filtering [16]. Assuming that $f(x,t)$ is the instantaneous variable of flow, in the physical space-time domain, the large-scale eddy can be expressed as

$$\overline{f}(x,t) = \int_D^{\overline{G}} (x, x', \Delta) f(x', t) \mathrm{d}x'. \tag{3}$$

In the formula, D is the computational domain of the flow field, x' and x represent the vectors before and after filtering, respectively, and G represents the filter function.

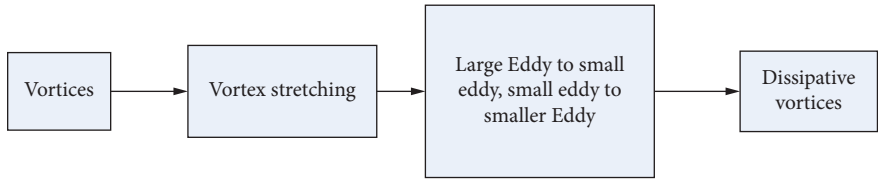

Figure 3: Cascade process of fluid energy.

The commonly used filter function $\overline{G}$ is divided into two categories: uniform filter and nonuniform filter [17, 18]. However, when carrying out the numerical simulation of wall turbulence, the normal grid in the near-wall area must be densified according to the proportional rules. Considering the two factors of calculation efficiency and accuracy, a nonuniform box filter is generally used [19], and its expression is

$$\overline{G}(\eta) = \begin{cases} \dfrac{1}{\Delta}, & |\Delta| \le \dfrac{\Delta}{2}, \\ \\ 0, & |\Delta| > \dfrac{\Delta}{2}. \end{cases} \tag{4}$$

In the formula, Δ is the scale of the filter, which can be understood as the scale requirement for the grid during numerical simulation. The difference between any grid nodes is

$$\eta = x_i - x_i'. \tag{5}$$

According to the above definition, the large-scale vortex $\overline{f}(x,t)$ is the average volume of the tetrahedron or hexahedron with x_i as the central node.

The filtered equation and the incompressible N–S equation are

$$\frac{\partial \overline{u}_i}{\partial x_i} = 0, \tag{6}$$

$$\frac{\partial \overline{u}_i}{\partial t} + \frac{\partial u_i \overline{u}_j}{\partial x_j} = -\frac{1}{\rho}\frac{\partial \overline{P}}{\partial x_i} + \nu \frac{\partial^2 \overline{u}_i}{\partial x_j^2} - \frac{\partial \tau_{ij}^s}{\partial x_j}. \tag{7}$$

$\overline{u}_i$ is the average velocity after filtering, and $\tau_{ij}^s = \overline{u_i u_j} - \overline{u_i}\,\overline{u_j}$ is the Reynolds stress at the sublattice scale.

The subgrid Reynolds stress τ_{ij}^s represents the interaction relationship between large and small scale vortices, and the cascade process of its turbulent energy is shown in Figure 3.

In order to explore the role of Reynolds stress in the cascade process, the Reynolds stress can be decomposed into

$$\tau_{ij} = L_{ij} + C_{ij} + R_{ij}. \tag{8}$$

Among them, L_{ij} is the Leonard stress term, C_{ij} is the cross stress term, and R_{ij} is the sublattice Reynolds stress, which represents the energy transfer of vortex systems of different sizes. Its mathematical derivation for the τ_{ij}^s modeling method is as follows.

Assuming that the generation and dissipation rates of turbulence are in equilibrium, the τ_{ij}^s is decomposed as

$$\tau_{ij}^s - \frac{1}{3}\delta_{ij}\tau_{kk} = 2\nu_T \overline{S}_{ij}. \tag{9}$$

In the formula, ν_T is the eddy viscosity coefficient of the sublattice scale; in order to satisfy the continuity equation of incompressible fluid, k exists if and only when $i = j$; δ_{ij} is the Kronecker number, and then,

$$\delta = \begin{cases} 0, & (i \ne j), \\ 1, & (i = j). \end{cases} \tag{10}$$

$\overline{S}_{ij}$ is the strain tensor at the Reynolds scale, and then,

$$\overline{S}_{ij} = \frac{1}{2}\left(\frac{\partial \overline{u}_i}{\partial x_j} + \frac{\partial \overline{u}_j}{\partial x_i}\right). \tag{11}$$

Since ν_T is an unknown coefficient about the flow field function, it is necessary to continue to seek a method for modeling the eddy-viscous coefficient [20]. Therefore, ν_T is a function of the velocity scale and length scale of the vortex, and the formula of the turbulent molecular viscosity coefficient is

$$\nu_T = C_D k_s \frac{1}{2}\Delta. \tag{12}$$

C_D is the coefficient, k_s is the turbulent pulsation kinetic energy, and Δ is the filter width.

As mentioned above, the dissipation term σ_s of turbulent energy, on the one hand, needs to be balanced with the dissipation rate, as follows:

$$2\nu_T \overline{S}_{\mathrm{ij}} \overline{S}_{\mathrm{ij}} = \sigma_S. \tag{13}$$

On the other hand, the dissipation term σ_s is related to the vortex scale and can be written as

$$\sigma_s = \frac{C_E {k_s}^{3/2}}{\Delta}. \tag{14}$$

Simultaneously, Formulas (12), (13), and (14) can be obtained:

$$2C_D {k_s}^{1/2} \Delta \overline{S}_{ij} \overline{S}_{ij} = \frac{C_E {k_s}^{3/2}}{\Delta}. \tag{15}$$

Then,

$$k_s = 2\frac{C_D}{C_E}\Delta^2 \overline{S}_{ij} \overline{S}_{ij}. \tag{16}$$

Substitute into Formula (12) to get:

$$\nu_T = C_D \Delta \sqrt{\frac{C_D}{C_E}} \Delta \sqrt{2\overline{S}_{ij}\overline{S}_{ij}}. \tag{17}$$

Then,

$$\nu_T = (C_S \Delta)^2 \sqrt{2\overline{S}_{ij}\overline{S}_{ij}}. \tag{18}$$

Among them, C_S is a dimensionless constant. In summary, the modeling results of the sublattice stress τ_{ij}^s are

$$\tau_{ij}^s - \frac{1}{3}\delta_{ij}\tau_{kk} = 2\nu_T \overline{S}_{ij} = 2(C_S\Delta)^2 \sqrt{2\overline{S}_{ij}\overline{S}_{ij}}\overline{S}_{ij}. \tag{19}$$

So far, the numerical equation of the large eddy simulation is obtained. In the process of simulating the flow field with LES, the appropriate sublattice model and fixed solution conditions are selected according to the specific situation, so as to obtain more realistic simulation results [21].

3.4. Simulation Calculation Results of the Flow Field of Sliding Bearing in Gear Pump. The theoretical radial leakage model and the theoretical end leakage model contain a dynamic viscosity term; that is, the flow leakage is related to the viscosity properties of the selected hydraulic oil. In fact, the fluid viscosity is also affected by temperature, and the viscosity would change due to the change in temperature. The effect of temperature needs to be added to refine the original leak model [22, 23]. At the same time, the fluid studied in this paper is an incompressible fluid, and its density remains constant and does not change with temperature. During operation, the pump body deforms, and the deformation of the pump body would affect the leakage to a certain extent. Moreover, under the condition of high pressure and high speed, if the strength of the pump body is insufficient, it would cause cracks or even burst.

The relationship between kinematic viscosity and temperature is generally expressed by the Walser equation:

$$\text{loglog}(v + a) = b - c \log T. \tag{20}$$

In the Formula, a, b, and c are constants related to the oil, and $a = 0.6$, b, and c are obtained by bringing the viscosity of the oil at two different temperatures into Formula (20). The hydraulic oil used in the gear pump experiment is generally #32 lubricating oil. The viscosity values at different temperatures are shown in Table 1. From the simulation results of the pump body deformation, it takes as many points as possible on the pump inner wall to check the position and its deformation and interpolates to fit the relationship between the circumferential position of the pump inner wall and the deformation. The gap between the tooth tip and the inner wall of the pump at a certain point is the sum of the determined radial gap and the deformation of the pump body at the position of the point, and the corresponding leakage is calculated according to different temperatures.

Taking the selection of #32 lubricating oil as an example, it is found from the calculation in Table 1 that the density of the lubricating oil is 850 kg/m^3. The effect of temperature on its density is negligible, which is consistent with the theoretical setting.

Table 1: #32 Oil temperature–viscosity data.

Temperature (°C)	Dynamic viscosity	Motion viscosity
22.8	83.29	97.97
32.4	46.32	54.48
40.6	28.63	33.66
50.3	20.11	23.67
61.3	14.11	16.58

4. Experiment of Circular Helical Gear Pump

4.1. Influence of Oil Inlet Pressure on Internal Flow Field of Sliding Bearing. This section analyzes the influence of the rated pressure of the oil inlet on the internal flow field characteristics of the sliding bearing when the eccentricity is fixed. For the internal flow field of the sliding bearing, the rotational speed is 10000 r/min. When the rated pressure of the oil inlet is 5 MPa, 10 MPa, 15 MPa, 20 MPa, 25 MPa, 30 MPa, and 35 MPa, respectively, the simulation analysis is carried out.

The correctness of the simulation results and the average flow rate obtained from the simulation of the tooth circular-arc wheel pump at the same speed with different loads and the same load with different speeds in the next rotation cycle are compared with the flow value obtained by theoretical calculation, as shown in Tables 2 and 3.

It can be seen from the data in Tables 2 and 3 that the flow value obtained by the simulation calculation is close to and slightly smaller than the theoretical flow rate, and the simulation calculation of the internal flow field of the gear pump is correct.

In order to more intuitively express the influence of the rated pressure of the oil inlet on the radial force balance ability, this paper mainly analyzes the difference between the pressure of the static pressure groove and the rated pressure of the oil inlet, as shown in Figure 4.

As can be seen from Figure 4(a), the greater the inlet pressure, the greater the pressure drop in the static pressure groove. When the rated pressure of the oil inlet is 35 MPa, the pressure drop of the static pressure tank reaches 9.7 MPa. The two sliding bearings can offset 49.52% of the radial force for the driven wheel with larger radial force, and when the oil inlet pressure is 5 MPa, it can offset 63.02%. It can be seen from Figure 4(b) that the greater the rated pressure of the oil inlet, the greater the radial force on the sliding bearing. As a result, the wear of the sliding bearing is more serious, the higher the temperature of the sliding bearing, the more serious the wear at the relative position of the oil inlet. When the rated pressure of the oil inlet is 5 MPa, the average temperature rise is about 16.012°C, and when the rated pressure of the oil inlet is 35 MPa, the average temperature rise reaches 23.85°C.

4.2. Improvement of Sliding Bearing in Gear Pump. During the actual operation of the high-performance small arc gear pump, due to its high pressure and high speed, the gear pump is small in volume, and the sealing area is small, and the sealing problem may also cause leakage. The front end cover of the gear pump is sealed with an O-ring to prevent leakage between the end face of the front end cover

Table 2: Comparison of simulated flow and theoretical flow with different loads.

Load (MPa)	No leakage theoretical flow (L/min)	There is leakage theoretical flow (L/min)	Simulation traffic (L/min)
5	20.0172	19.6012	19.3807
15	20.0172	19.2499	19.0127
20	20.0172	19.0023	18.9935
25	20.0172	18.9238	18.001

Table 3: Comparison of simulated flow and theoretical flow at different speeds.

Rotational speed (r/min)	No leakage theoretical flow (L/min)	There is leakage theoretical flow (L/min)	Simulation traffic (L/min)
4000	8.00684	7.2657	7.0723
10000	20.0172	19.2489	19.0129
12000	24.0206	22.9274	22.6507

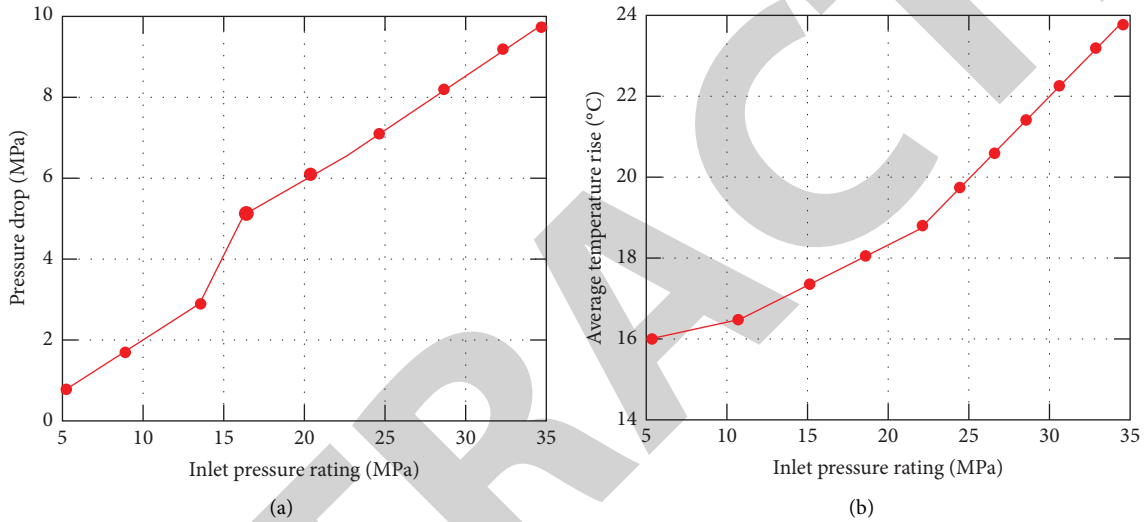

Figure 4: Influence of oil inlet pressure on pressure drop in static pressure tank and average bearing temperature rise (a). Influence of oil inlet pressure on pressure drop in static pressure groove (b). Influence of oil inlet pressure on average bearing temperature rise.

and the pump body, and an oil seal is installed at the through hole to prevent leakage between the drive gear shaft and the end cover. Setting the rated pressure of the internal flow field of the sliding bearing to 25 MPa, when the rotation speed is 10000°r/min, simulation analysis is carried out for different oil inlet position angles, and the influence of oil inlet position angles on the pressure and temperature rise of the static pressure tank is discussed. The location of the oil inlet with the most positive impact on the overall performance is determined, which takes into account the structural characteristics of the plain bearing, and the range of the position angle is selected from the angle between the oil inlet and the horizontal direction of 40° to 70°, as shown in Figure 5.

As can be seen in Figure 5(a), the position angle of the oil inlet increases, and the pressure of the static pressure tank decreases, and this would lead to a worsening effect of balancing the radial force, but the effect is not very large. When the position angle is 40°, the pressure of the hydrostatic groove is 17.8 MPa, and the two sliding bearings can offset 51.92% of the radial force for the driven wheel with a larger radial force. When the position angle is 70°, the pressure of the hydrostatic groove is 17.24 MPa, which can offset 50.31% of the radial force. As shown in Figure 5(b), under the combined influence of the dynamic pressure, eccentricity, and static pressure groove pressure generated during the operation of the sliding bearing, as the oil inlet position angle increases, the temperature rise of the fluid inside the sliding bearing first decreases and then increases. It reaches a minimum value at 47°. Therefore, through the comprehensive conclusion, it is more appropriate to select 47° for the position angle of the oil inlet of the sliding bearing.

In order to more accurately analyze the influence of the oil inlet diameter on the flow field performance of the sliding bearing, from 1.25 mm to 3.85 mm, simulation analysis is carried out for every 2 mm increase, as shown in Figure 6.

As can be seen from Figure 6(a), the diameter of the oil inlet increases, and the width of the oil passage increases. The increase in the amount of high-pressure oil feed increases the pressure of the hydrostatic groove, so the effect of balancing the radial force in the hydrostatic groove becomes better, but the increase in the pressure of the hydrostatic groove tends to slow down. When the diameter of the oil inlet is 1.25 mm, the pressure of the static pressure groove is 8.79 MPa, and the two sliding bearings can only offset 25.78% of the radial force for the driven wheel with a large radial force. When the diameter is 3.85 mm, the pressure of the hydrostatic groove

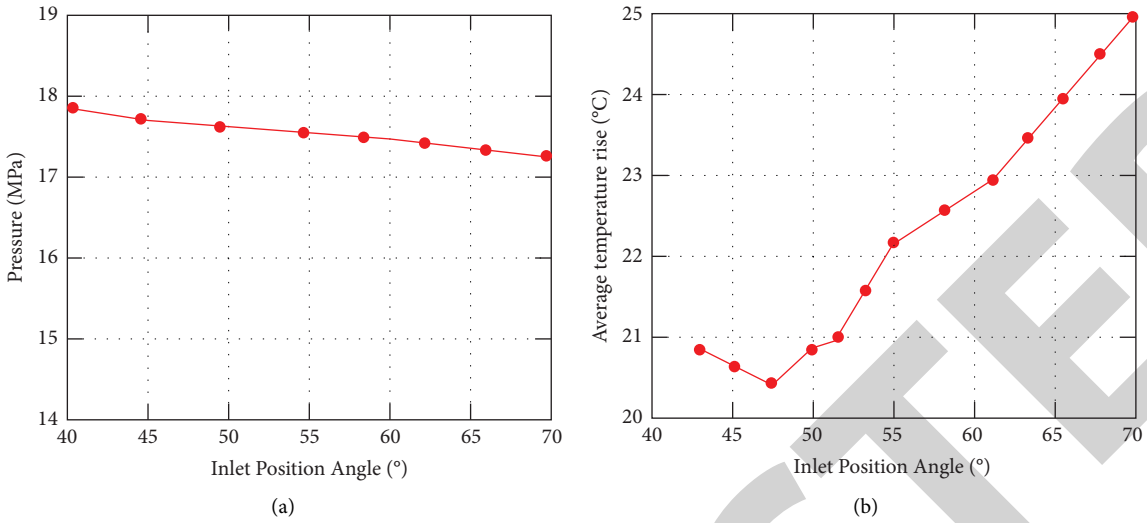

Figure 5: The influence of the position angle of the oil inlet on the pressure and temperature rise of the static pressure tank (a). Effect on static pressure tank pressure (b). Effect on average temperature rise.

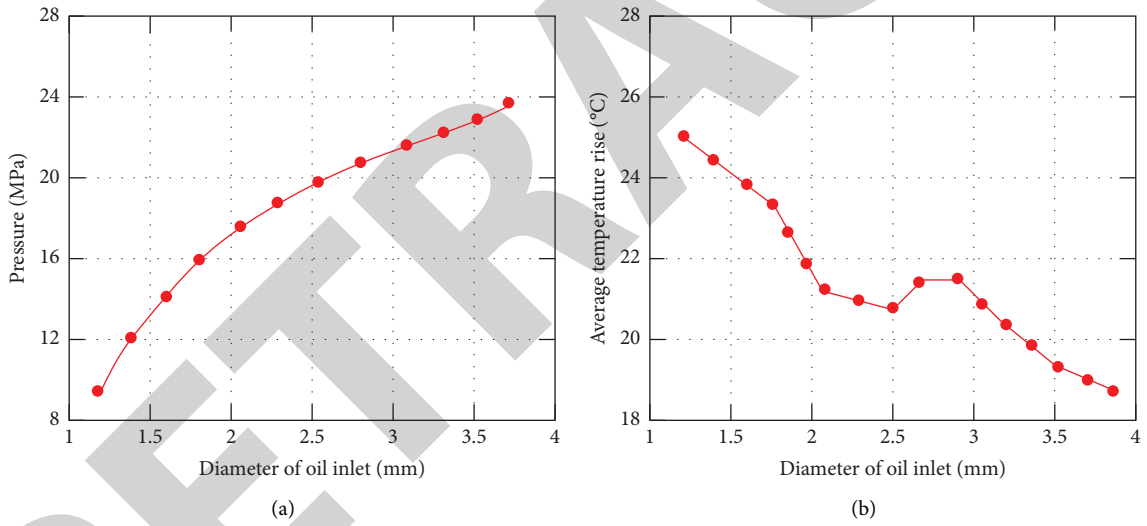

Figure 6: Influence of inlet diameter on pressure and temperature rise in hydrostatic tank (a). Effect on static pressure tank pressure (b). Effect on average temperature rise.

is 23.8 MPa, which can offset 67.50% of the radial force. It can be seen from Figure 6(b) that the diameter of the oil inlet increases, the high pressure oil pours in a lot, and the pressure on the gear shaft increases, which would lead to an increase in the eccentricity. The maximum temperature rise of the sliding bearing oil film increases, and a large influx of hydraulic oil would also take away a lot of heat. Therefore, the average temperature rise shows an overall trend of decreasing but fluctuates from 2.1 mm to 3.1 mm. When the diameter of the oil inlet is 1.25 mm, the average temperature rise is 25.5°C, and when the diameter is 3.85 mm, the average temperature rise is 18.5°C. As far as the overall trend is concerned, the increase in the diameter of the oil inlet has a positive effect on reducing the pressure drop in the static pressure tank and reducing the temperature rise. However, if the diameter of the oil inlet is too large, the flow rate of the sliding bearing would increase greatly, which would increase the leakage of the gear pump, and taking into account the average temperature rise between 2.4 mm and 3.1 mm, the final choice for the diameter of the oil inlet is 2.4 mm.

4.3. Temperature Test Experiment of Arc Helical Gear Pump. In order to study the temperature rise characteristics of the arc helical gear pump during operation, it avoids the viscosity of the lubricating oil overheating caused by the operation of the arc helical gear pump under high pressure and high speed conditions. It leads to problems such as serious wear and increased leakage, and to analyze the influence of the sliding bearing optimization on the temperature rise

characteristics of the gear pump, the experimental test and analysis of the temperature rise characteristics of the gear pump were carried out.

4.3.1. Influence of Sliding Bearing Optimization on Temperature Rise of Gear Pump Prototype. When the sliding bearings in the gear pump prototype are, respectively, without hydrostatic grooves, before optimization, and after optimization, they run for 600°s under the condition of speed of 2100°r/min and load of 8 MPa. The relationship between the surface temperature rise of the gear pump and the operating time was obtained. After each experimental operation, it needs to be stopped for 30 minutes to wait for the gear pump prototype and hydraulic oil to cool down. After the test, it was found that the temperature rise at the T2 position was the highest, so the relationship between the temperature rise of T2 and the time was plotted, as shown in Figure 7.

It can be seen from Figure 7 that the optimization of the sliding bearing has an obvious effect on the improvement of the temperature rise of the gear pump. It runs for 600°s under the working conditions of the speed of 2100°r/min and the load of 8 MPa. The surface temperature rise of the gear pump with optimized sliding bearings is reduced by about 2.5°C. Compared with the ordinary plain bearing without hydrostatic groove, the surface temperature rise of the gear pump prototype with the optimized plain bearing is reduced by about 12°C. In general, the optimized sliding bearing has significant advantages in reducing the temperature rise of high-performance small arc helical gear pumps. It also proves that the optimization of the sliding bearing is the key to improving the temperature rise of the gear pump.

4.3.2. The Influence of the Optimized Sliding Bearing on the Flow Rate of the Gear Pump Prototype. By analyzing the leakage phenomenon of the gear pump after the optimization of the arc helical gear bearing, in order to test the accuracy of the hydraulic oil temperature rise and the pump flow leakage model, the flow characteristics of the gear pump were analyzed, and the flow characteristics of the gear pump were experimentally tested and analyzed. When the sliding bearings in the gear pump prototype are the sliding bearings before optimization and the sliding bearings after optimization, the relationship between the speed and flow of the gear pump prototype is tested when the load is 8 MPa, as shown in Figure 8. In the measurement range, with the increase of rotational speed, the flow rate of the gear pump increases, which is linear.

It can be seen from Figure 8 that the optimized sliding bearing reduces the flow leakage of the gear pump. This advantage is not obvious when the speed is lower than 2500°r/min. With the increase of rotational speed, it can be seen that the volumetric efficiency of the optimized sliding bearing gear pump is significantly higher than that of the gear pump before optimization. It can be obtained by calculation that when the arc gear pump runs under the working condition of the load of 10 MPa, within the tested speed range, the volumetric efficiency of the gear pump is the highest at 15000°r/min, reaching 64.43%. The volumetric

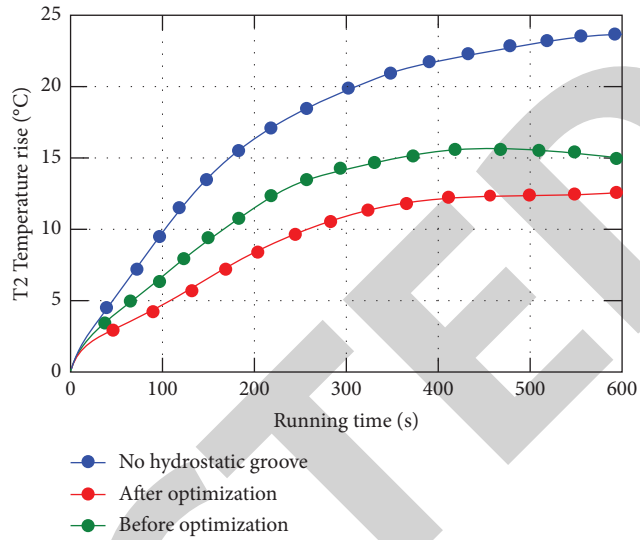

Figure 7: Temperature rise of gear pump with different plain bearings installed.

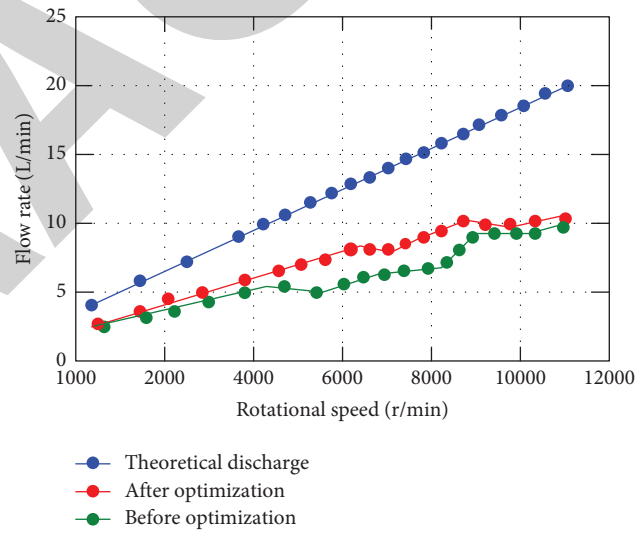

Figure 8: Flow rate of gear pump at different speeds before and after sliding bearing optimization.

efficiency is also relatively low when the rotational speed is low, and the volumetric efficiency of the gear pump is 53.71% at 1100°r/min. The higher the rotation speed, the higher the volumetric efficiency; that is, the higher the rotation speed, the smaller the leakage, and the higher the volumetric efficiency. Before the optimization of the sliding bearing, the volumetric efficiency of the gear pump was at least 49.81% at 1700°r/min and 60.16% at 15000°r/min. Overall, the volumetric efficiency of the gear pump increases after the sliding bearing is optimized. The volumetric efficiency of the gear pump is the ratio of the actual flow to the theoretical flow.

4.3.3. Comparison of Theoretical Flow and Actual Flow. The leakage model is compared with the actual leakage through flow experiments to verify the correctness of the

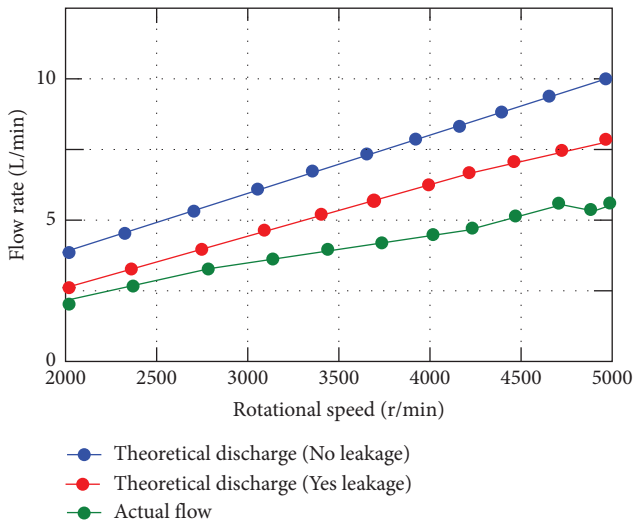

Figure 9: Theoretical and actual flow at different speeds.

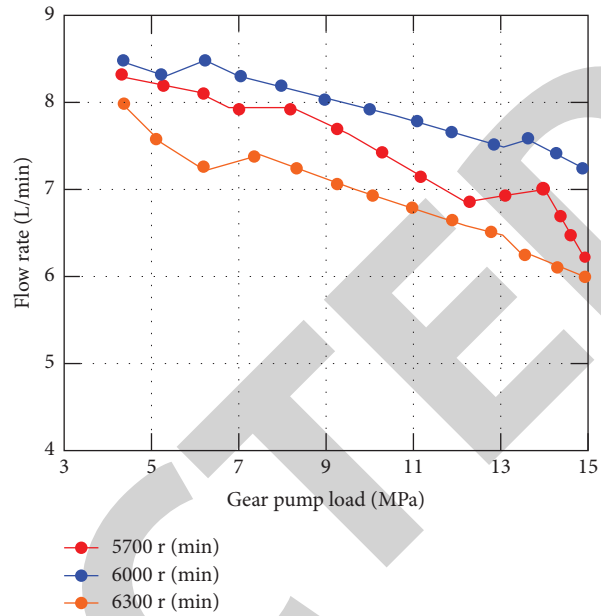

Figure 10: Effect of gear pump load on flow at different speeds.

theoretical leakage model. According to the temperature rise of different speeds obtained from the simulation, the load and other related parameters of the sliding bearing calculated by the simulation are brought into the program. When the load is 8 MPa, the relationship between the flow rates at different speeds of the gear pump prototype is tested, as shown in Figure 9.

It can be seen from Figure 9 that the flow calculation results of the theoretical model including leakage are closer to the actual flow, but there is still a certain gap. Due to the wear of the gear pump when it is running at high pressure and high speed, the leakage is aggravated. At the same time, the wear and tear generated during the actual loading operation make the temperature of the hydraulic oil rise greatly, which is also the reason for the large amount of leakage. The lower the rotational speed, the smaller the difference between the theoretical flow with leakage and the actual flow. The existing formula is more suitable for low speed. For high-speed operation, the basic leakage theoretical model can be further studied.

4.3.4. The Influence of Load on the Flow Rate of the Gear Pump Prototype. When the rotational speed of the arc helical gear pump is 5700°r/min, 6000°r/min, and 6300°r/min, respectively, it starts loading from no-load and collects the flow signal of the gear pump within the load range from 5.8 MPa to 14.8 MPa. The test results of the gear pump flow experiment are shown in Figure 10.

In Figure 10, as the load of the gear pump increases, the flow rate of the gear pump shows an overall trend of decreasing. Since the theoretical flow rate of the gear pump is constant at the same speed, the higher the load, the lower the volumetric efficiency. The higher the load, the larger the leakage, and the lower the volumetric efficiency. The accuracy of the flow leakage model and the simulation calculation of the dynamic performance of the internal flow field of the gear pump are verified.

5. Conclusion

In this paper, based on the background of machine learning, the three-dimensional flow field simulation and sound field source simulation of the flow field in the arc helical gear pump are carried out. The difference in the flow in the pump under different working conditions is analyzed, and the dynamic performance simulation of the gear pump is deeply studied. Aiming at the flow leakage problem of the arc helical gear pump, a flow leakage model of the gear pump is established. It solves the problem of obvious temperature rise of the sliding bearing in the gear pump and serious wear caused by the large radial force. Through experimental analysis, the surface temperature rise of the gear pump optimized by the sliding bearing is reduced by about 2.5°C when the speed is 2100°r/min for 600°s. Compared with ordinary plain bearings, the surface temperature rise is reduced by about 12°C. It is concluded that the optimization of the sliding bearing has an obvious improvement effect on the temperature rise of the gear pump. It proves that the arc helical gear pump can run smoothly under high pressure and high speed compared with other ordinary gear pumps. The application of the proposed helical gear pump simulation method in this paper is relatively shallow in research and analysis, and it still needs to be further improved. It is also possible to try to simulate various errors in the processing of the gear pump. In view of the leakage problem of the helical gear pump, the sealing materials and methods of the gear pump under high pressure conditions are studied, the compensation method of the gear pump is improved, and the leakage problem at high pressure and high speed is improved. Through simulation and experiment, it is found that the optimization of sliding bearing has a significant effect on reducing temperature rise and balancing radial force, so the sliding bearing in gear pump needs to be further optimized.

Data Availability

The data of this paper can be obtained through the e-mail to the authors.

Conflicts of Interest

The authors declare that there are no conflicts of interest regarding the publication of this work.

References

[1] A. Buczak and E. Guven, "A survey of data mining and machine learning methods for cyber security intrusion detection," *IEEE Communications Surveys & Tutorials*, vol. 18, no. 2, pp. 1153–1176, 2017.

[2] L. Zhou, S. Pan, J. Wang, and A. V. Vasilakos, "Machine learning on big data: opportunities and challenges," *Neurocomputing*, vol. 237, no. 10, pp. 350–361, 2017.

[3] I. Kavakiotis, O. Tsave, A. Salifoglou, N. Maglaveras, I. Vlahavas, and I. Chouvarda, "Machine learning and data mining methods in diabetes research," *Computational and Structural Biotechnology Journal*, vol. 15, no. C, pp. 104–116, 2017.

[4] E. Merzari, H. Yuan, A. Kraus et al., "High-fidelity simulation of flow-induced vibrations in helical steam generators for small modular reactors," *Nuclear Technology*, vol. 205, no. 1-2, pp. 33–47, 2019.

[5] W. Xu, Y. Yu, E. Wang, and L. Zhou, "Flow-induced vibration (FIV) suppression of two tandem long flexible cylinders attached with helical strakes," *Ocean Engineering*, vol. 169, no. 1, pp. 49–69, 2018.

[6] L. K. Quen, A. Abu, N. Kato, P. Muhamad, L. K. Tan, and H. S. Kang, "Performance of two- and three-start helical strakes in suppressing the vortex-induced vibration of a low mass ratio flexible cylinder," *Ocean Engineering*, vol. 166, no. 15, pp. 253–261, 2018.

[7] H. Ren, Y. Xu, J. Cheng et al., "Vortex-induced vibration of flexible pipe fitted with helical strakes in oscillatory flow," *Ocean Engineering*, vol. 189, no. 1, pp. 1–15, 2019.

[8] W. Xu, C. Ji, H. Sun, W. Ding, and M. M. Bernitsas, "Flow-induced vibration of two elastically mounted tandem cylinders in cross-flow at subcritical reynolds numbers," *Ocean Engineering*, vol. 173, no. 1, pp. 375–387, 2019.

[9] S. Li, N. Chu, P. Yan, D. Wu, and J. Antoni, "Cyclostationary approach to detect flow-induced effects on vibration signals from centrifugal pumps," *Mechanical Systems and Signal Processing*, vol. 114, no. 1, pp. 275–289, 2019.

[10] C. Wang, W. Jiang, Y. Yue, and S. Zhang, "Research on prediction method of gear pump remaining useful life based on DCAE and Bi-LSTM," *Symmetry*, vol. 14, no. 6, p. 1111, 2022.

[11] J. X. Wang, J. L. Wu, and H. Xiao, "Physics-informed machine learning approach for reconstructing reynolds stress modeling discrepancies based on DNS data," *Physical Review Fluids*, vol. 2, no. 3, pp. 1–22, 2017.

[12] A. N. A. Al-Masri and H Mokayed, "Intelligent fault diagnosis of gears based on deep learning feature extraction and particle swarm support vector machine state recognition," *Journal of Intelligent Systems and Internet of Things*, vol. 4, no. 1, pp. 26–40, 2021.

[13] H. Chen, Y. Lu, and L. Tu, "Fault identification of gearbox degradation with optimized wavelet neural network," *Shock and Vibration*, vol. 20, no. 2, pp. 247–262, 2013.

[14] M. Battarra and E. Mucchi, "On the assessment of lumped parameter models for gear pump performance prediction," *Simulation Modelling Practice and Theory*, vol. 99, Article ID 102008, 2020.

[15] L. Gao, X. Hu, W. Liu, and D. Sun, "Study on wear mechanism of gear pump end plate of combined harvester based on CFD fluid analysis," *Concurrency and Computation: Practice and Experience*, vol. 31, no. 10, Article ID e4711, 2019.

[16] X. Li, L. Tang, and M. Qian, "Steady-state flow characteristics and end clearance optimization of internal gear grease pump," *Advances in Materials Science and Engineering*, vol. 2021, Article ID 8293040, 16 pages, 2021.

[17] A. Zhou, L. Zhai, Z. Zhu, J. Guo, X. Zhang, and B. Cui, "Effects of transmission ratio on the nonlinear vibration characteristics of a gear-driven high-speed centrifugal pump," *Shock and Vibration*, vol. 2021, Article ID 6629241, 15 pages, 2021.

[18] S. Guo and D. Chen, "Calculation of unloading area of internal gear pump and optimization," *Mathematical Problems in Engineering*, vol. 2020, Article ID 7319871, 9 pages, 2020.

[19] Z. Wang, X. He, H. Shen, S. Fan, and Y. Zeng, "Multi-source information fusion to identify water supply pipe leakage based on SVM and VMD," *Information Processing & Management*, vol. 59, no. 2, Article ID 102819, 2022.

[20] D. Chen, W. Chen, Y. Xu et al., "Upregulated immune checkpoint HHLA2 in clear cell renal cell carcinoma: a novel prognostic biomarker and potential therapeutic target," *Journal of Medical Genetics*, vol. 56, no. 1, pp. 43–49, 2019.

[21] B. L. Da Silva, R. D. Luciano, J. Utzig, and H. F. Meier, "Analysis of flow behavior and fluid forces in large cylinder bundles by numerical simulations," *International Journal of Heat and Fluid Flow*, vol. 75, pp. 209–226, 2019.

[22] B. Zhao, "The application of wavelet finite element method on multiple cracks identification of gear pump gear," *Engineering with Computers*, vol. 31, no. 2, pp. 281–288, 2015.

[23] X. Bai, Z. Le, and Y. Zhang, "Effect of mass ratio on energy capture efficiency of vibration induced by cylinder flow," *Acta Energiae Solaris Sinica*, vol. 39, no. 12, pp. 3325–3330, 2018.